PCCP

PAPER

View Article Online
View Journal | View Issue

Cite this: *Phys. Chem. Chem. Phys.*, 2022, **24**, 29655

Spectroscopic investigation of photophysics and tautomerism of amino- and nitroporphycenes†

Idaresit Mbakara,[a] Agnieszka Gajewska,[a] Arkadiusz Listkowski,[ab] Michał Kijak,[a] Krzysztof Nawara,[ab] Tatu Kumpulainen,‡[c] Eric Vauthey[c] and Jacek Waluk*[ab]

Received 29th September 2022,
Accepted 22nd November 2022

DOI: 10.1039/d2cp04555a

rsc.li/pccp

Parent, unsubstituted porphycene and its two derivatives: 2,7,12,17-tetra-*n*-propylporphycene and 2,7,12,17-tetra-*t*-butylporphycene were substituted at the *meso* position with amino and nitro groups. These two families of porphycenes were characterized in detail with respect to their spectral, photophysical, and tautomeric properties. Two *trans* tautomers of similar energies coexist in the ground electronic state, but only one form dominates in the lowest excited singlet state. Absorption, magnetic circular dichroism (MCD), and emission anisotropy combined with quantum-chemical calculations led to the assignment of S_1 and S_2 transitions in both tautomers. Compared with the parent porphycene, the S_1–S_2 energy gap significantly increases; for one tautomeric form, the effect is twice as large as for the other. Both amino- and nitroporphycenes emit single fluorescence; previously reported dual emission of aminoporphycenes is attributed to a degradation product. Introduction of bulky *t*-butyl groups leads to a huge decrease in fluorescence intensity; this effect, arising from the interaction of the *meso* substituent with the adjacent *t*-butyl moiety, is particularly strong in the nitro derivative.

Introduction

Porphycene (**Pc**), the first reported constitutional isomer of porphyrin,[1] is an important molecule for fundamental research and various possible applications. Spectral and photophysical parameters of porphycenes, such as strong absorption in the red part of the visible range and considerable triplet population yield, make this class of compounds promising agents in photodynamic therapy of cancer[2] or photoinactivation of microbes.[3,4] Other possible uses include application of porphycenes as artificial heme components,[5] building blocks in molecular electronics,[6] catalysts,[7–10] or liquid crystals.[11]

Regarding fundamental studies, porphycenes have been widely utilized as model systems for intramolecular hydrogen bond (HB) and tautomerism involving single or double hydrogen transfer.[12] The rectangular shape of the inner cavity composed of four nitrogen atoms leads to strong HBs, and, in consequence, low tautomerization barriers. Under such conditions, tautomerization in solution is very fast (femto- and picoseconds);[13] moreover, it is governed by tunneling, both "deep" (occurring from the vibrational ground state) and thermally activated after excitation of specific vibrational modes.[14] Tautomerization in porphycenes has been studied in various experimental regimes: ensemble studies in condensed phases,[13–24] investigations of ultracold molecules isolated in supersonic jets[25,26] or helium nanodroplets,[27] and, finally, single molecule techniques involving fluorescence,[28–31] Raman,[32,33] and scanning probe microscopy.[34–40]

It has been demonstrated that photophysics of porphycenes and their tautomeric properties are strongly related. Even though most porphycene derivatives are good or moderate emitters, some spectacular exceptions have been reported. For instance, substitution with alkyl groups at the four *meso* positions (9,10,19,20-) lowers the fluorescence quantum yield by three orders of magnitude,[20] whereas 9,20-doubly substituted porphycenes do not reveal such an effect.[24] Fluorescence can be recovered by placing the chromophore in a rigid environment,[20] which suggests that rapid S_1 radiationless deactivation involves a large amplitude geometry distortion. A good correlation was found between the fluorescence quantum yield of porphycenes and the distance between the nitrogen atoms linked by the intramolecular H-bond.[23] The latter is a reliable measure of the HB strength. Similar behavior has been reported for other porphycenes.[41]

[a] *Institute of Physical Chemistry, Polish Academy of Sciences, 01-224 Warsaw, Kasprzaka 44/52, Poland. E-mail: jwaluk@ichf.edu.pl*
[b] *Faculty of Mathematics and Science, Cardinal Stefan Wyszyński University, Dewajtis 5, 01-815 Warsaw, Poland*
[c] *Physical Chemistry Department, Sciences II, University of Geneva, 30, Quai Ernest Ansermet, CH-1211 Geneva 4, Switzerland*

† Electronic supplementary information (ESI) available. See DOI: https://doi.org/10.1039/d2cp04555a

‡ Present address: Department of Chemistry/Nanoscience Center, University of Jyväskylä, Survontie 9 C, 40014, Jyväskylä, Finland.

Interestingly, large changes in photophysics caused by modification of the geometry of the inner cavity can be induced even by "mild" substituents, *e.g.*, fluorine or alkyl. This raises a question of the influence on the photophysics of strong electron donating and electron accepting substituents, such as amino or nitro groups. Several amino-substituted porphycenes have been reported in the literature.[19,42–45] Nonell and coworkers studied 9-amino derivatives of porphycenes tetra-substituted at the β positions (2,7,12,17-) with phenyl,[19,43,44] propyl,[45] or methoxyethyl[45] moieties. They reported dual fluorescence, which was attributed to two *trans* tautomeric forms. Different decay times (in the range of a few nanoseconds), as well as different excitation spectra, indicated lack of excited state equilibrium between the two excited species. In particular, slow excited state tautomerization from the higher energy form was a rather unexpected result, given the rates previously reported for other porphycenes.

Nitro-substituted porphycenes have not been explored much. Absorption spectra are available for 9-nitro-2,7,12,17-tetra-*n*-propylporphycene[46] and 9-nitro-2,7,12,17-tetraphenylporphycene,[43] and 9-acetoxy-19-nitro-2,7,12,17-tetra-*n*-propylporphycene.[46] Arad *et al.* reported a single emission of 9-nitro-2,7,12,17-tetraphenyl porphycene.[43] Interestingly, while the decay time of 3.9 ns is only 2.5 times shorter than that reported for bare porphycene in the same solvent (toluene), the difference in fluorescence quantum yield is dramatic: the emission is 15 times stronger in the parent, unsubstituted compound.

The photophysical data reported for 9-aminoporphycenes bearing different substituents at the β positions indicate that the photophysical parameters can be strongly affected by the substituents. For example, fluorescence quantum yield in toluene is over an order of magnitude stronger in the tetrapropyl derivative[42] than in the tetraphenyl analogue[43] (0.06 *vs.* 0.004, respectively). Therefore, in order to accurately determine the influence of nitro and amino derivatives, singly substituted porphycenes are required. This was our motivation for the present work. We have synthesized 9-aminoporphycene (**APc**) and 9-nitroporphycene (**NPc**), as well as their corresponding 2,7,12,17-tetra-*n*-propyl derivatives (**tprAPc** and **tprNPc**, respectively), and determined their spectral and photophysical parameters. In order to assess the additional role of bulky substituents at the β positions on the spectra and photophysical parameters, tetra-*t*-butyl analogs of **APc** and **NPc** (**ttAPc** and **ttNPc**, respectively, see Scheme 1) have also been investigated and characterized. Combination of the experimental results with DFT modeling was used to understand the spectral and tautomeric properties of these two classes of compounds.

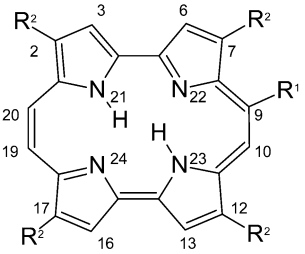

R^1	R^2	
H	H	**Pc**
H	*t*-Bu	**ttPc**
NH_2	H	**APc**
NH_2	*n*-Pr	**tprAPc**
NH_2	*t*-Bu	**ttAPc**
NO_2	H	**NPc**
NO_2	*n*-Pr	**tprNPc**
NO_2	*t*-Bu	**ttNPc**

Scheme 1 Structures of porphycenes and the acronyms used.

Results

Theoretical predictions of the relative energies of tautomeric forms

Six possible tautomeric forms are possible for porphycenes (Scheme 2), pairwise degenerate in **Pc** and **ttPc**, but not in the 9-substituted derivatives. While discussing relative stabilities in the ground state, we do not take into account the nonplanar *cis*3 and *cis*4 forms, whose energy is estimated to be much higher. DFT calculations predict that in the ground electronic state the two lowest energy forms in both amino and nitro derivatives are nearly degenerate: two *trans* tautomers are separated by less than 0.5 kcal mol^{-1} (Tables 1 and 2). One should note, however, that the predicted energy ordering changes: the lowest energy tautomeric species correspond to *trans*1 and *trans*2 in the amino and nitro derivatives, respectively. Upon excitation to S_1, the *trans*2–*trans*1 energy difference becomes large, more than ten times that of S_0 for the **APc** and five times for **NPc**. Moreover, the *cis*2 form of **APc** and the *cis*1 form of **NPc** are calculated for S_1 at a lower energy than that of the less stable *trans* species. One should therefore consider a possible presence of the *cis* species, in particular in the lowest excited state.

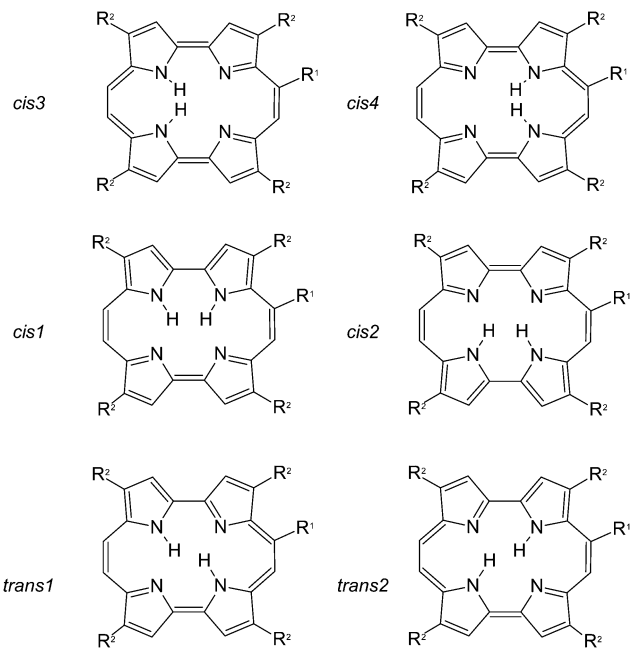

Scheme 2 Possible tautomeric forms.

Table 1 Calculated relative energies (kcal mol^{-1}) and permanent dipole moments of the tautomeric forms of porphycene (**Pc**), 9-aminoporphycene (**APc**), and 9-nitroporphycene (**NPc**)

	S_0[a]	S_1[b]	$\mu(S_0)$ [D]	$\mu(S_1)$[bc] [D]
Pc				
trans	0.00 (0.00)	0.00 (0.00)	0.00	0.00
		0.00 (0.00)		
cis	2.30 (1.74)	1.99 (1.67)	1.31	1.20
		2.13 (1.55)		
APc				
*trans*1	0.00 (0.00)	0.00 (0.00)	2.30	3.63
		0.00 (0.00)		3.14
*trans*2	0.28 (0.24)	3.20 (2.69)	2.47	3.79
		3.01 (2.37)		3.39
*cis*1	2.03 (1.51)	5.54 (4.36)	2.99	3.95
		5.40 (4.22)		3.45
*cis*2	2.55 (1.91)	2.01 (1.67)	2.40	3.72
		2.15 (1.77)		3.63
NPc				
*trans*1	0.42 (0.37)	2.35 (2.08)	6.54	6.77
		2.12 (2.00)		6.38
*trans*2	0.00 (0.00)	0.00 (0.00)	6.85	8.68
		0.00 (0.00)		7.70
*cis*1	2.60 (1.98)	2.29 (1.85)	6.66	8.23
		2.43 (1.98)		7.06
*cis*2	2.16 (1.64)	3.76 (3.10)	7.05	7.72
		3.78 (2.90)		7.67

[a] In parentheses, ZPVE-corrected values. [b] First row, B3LYP/6-31+G(d,p), second row, CAM-B3LYP/6-31+G(d,p) results. [c] Calculated for the optimized S_1 geometries.

Table 2 Calculated relative energies (kcal mol^{-1}) and permanent dipole moments of the tautomeric forms of 2,7,12,17-tetra-*t*-butyl substituted porphycene (**ttPc**), 9-aminoporphycene (**ttAPc**), and 9-nitroporphycene (**ttNPc**)

	S_0[a]	S_1[b]	$\mu(S_0)$ [D]	$\mu(S_1)$[bc] [D]
ttPc				
trans	0.00 (0.00)	0.00 (0.00)	0.00	0.00
		0.00 (0.00)		0.00
cis	2.07 (1.53)	1.68 (1.28)	1.44	1.19
		1.90 (1.28)		1.63
ttAPc				
*trans*1	0.00 (0.00)	0.00 (0.00)	2.09	3.04
		0.00 (0.00)		2.50
*trans*2	0.06 (0.00)	3.22 (2.82)	2.40	3.41
		3.06 (2.88)		3.03
*cis*1	1.63 (1.14)	5.26 (4.21)	2.98	3.39
		5.29 (4.16)		3.11
*cis*2	2.10 (1.53)	1.69 (1.50)	2.39	3.14
		1.90 (1.65)		3.03
ttNPc				
*trans*1	-0.01 (0.04)	−0.55 (−0.69)	6.91	7.96
		0.12 (−0.07)		7.39
*trans*2	0.00 (0.00)	0.00 (0.00)	6.89	8.43
		0.00 (0.00)		7.61
*cis*1	2.20 (1.72)	1.84 (1.34)	6.66	8.12
		1.96 (1.36)		7.24
*cis*2	1.51 (1.15)	1.40 (0.88)	7.32	8.49
		1.70 (1.06)		8.39

[a] In parentheses, ZPVE-corrected values. [b] First row, B3LYP/6-31+G(d,p), second row, CAM-B3LYP/6-31+G(d,p) results. [c] Calculated for the optimized S_1 geometries.

According to the theoretical predictions, adding four propyl groups at the β positions does not lead to significant changes in the relative tautomer energies and their dipole moments (Table S1, ESI†). Also the calculations performed for the *t*-butyl derivatives yield for **ttAPc** the same pattern as for **APc**. Interestingly, for **ttNPc** the theory suggests that the two *trans* species retain similar energies in S_1.

Absorption and MCD spectra

Aminoporphycenes. Since the two lowest energy forms – *trans*1 and *trans*2 tautomers – are predicted to be nearly degenerate, one can expect that the absorption should correspond to the sum of approximately equal contributions from both species. Calculations of the transition energies in the region of Q bands (S_1 and S_2 states, Table 3) indicate that the lowest energy band should correspond to the absorption from *trans*1, followed by a somewhat stronger transition from *trans*2, located *ca.* 900 cm^{-1} higher. The opposite pattern is obtained for the absorption to the second excited singlet electronic state. Now, the lower energy, weaker transition should occur from *trans*2, whereas the corresponding band of *trans*1 is expected to lie about 700 cm^{-1} higher.

Parent porphycene and 2,7,12,17-tetraalkyl-substituted derivatives exhibit a characteristic absorption pattern, consisting of three main bands in the Q region. The lowest energy band corresponds to the origin of the S_1 transition, the highest energy one to a vibronic feature of S_2, while the middle band contains contributions from the origin of S_2 and the vibronic transitions of S_1. These contributions could be distinguished by measuring the spectra in rare gas matrices.[47] One can therefore expect for **APc** a quite complex absorption pattern, consisting of (possibly overlapping) features due to different tautomers and different electronic states. In order to reliably assign the electronic transitions observed in absorption, we combined two

Table 3 Calculated transition energies (cm^{-1}) and oscillator strengths (in parentheses) of the tautomeric forms of **Pc**, **APc**, and **NPc**

	$S_1 \leftarrow S_0$[a]	$S_1 \rightarrow S_0$[b]	$S_2 \leftarrow S_0$[a]
Pc			
trans	17 904 (0.13)	17 084 (0.15)	18 804 (0.21)
		16 649 (0.22)	
cis	17 935 (0.14)	16 883 (0.16)	18 804 (0.18)
		16 638 (0.23)	
APc			
*trans*1	15 792 (0.18)	14 801 (0.18)	18 810 (0.16)
		14 621 (0.23)	
*trans*2	16 718 (0.25)	15 904 (0.25)	18 081 (0.10)
		15 733 (0.33)	
*cis*1	16 927 (0.22)	16 133 (0.22)	18 435 (0.13)
		16 054 (0.30)	
*cis*2	15 746 (0.17)	14 491 (0.17)	18 375 (0.14)
		14 183 (0.23)	
NPc			
*trans*1	17 616 (0.09)	16 560 (0.12)	18 126 (0.12)
		16 433 (0.19)	
*trans*2	17 085 (0.10)	15 876 (0.10)	18 464 (0.19)
		15 986 (0.15)	
*cis*1	17 146 (0.11)	15 603 (0.12)	18 160 (0.17)
		15 692 (0.18)	
*cis*2	17 559 (0.09)	16 466 (0.10)	18 414 (0.09)
		16 718 (0.16)	

[a] Optimized S_0 geometry. [b] Optimized S_1 geometry, first row: B3LYP/6-31+G(d,p), second row: CAM-B3LYP/6-31+G(d,p).

techniques that rely on polarized light: magnetic circular dichroism (MCD) and fluorescence anisotropy. For the assignments of electronic transitions, MCD spectroscopy is of great help. Porphycenes are "hard" chromophores,[48] of which the (+,−) MCD signal pattern of the lowest two electronic transitions is retained upon substitution or intramolecular tautomerization. Therefore, a positive/negative MCD sign indicates the S_1/S_2 absorption, independent of which tautomer it comes from. Moreover, MCD allows to separate the vibronic components of S_1 from the origin of S_2, since the vibronic features usually exhibit the same MCD sign as the electronic origin.

Using emission anisotropy, we exploit two characteristic features of the transition moments in porphycenes: (a) for each of *trans* tautomers, the S_0–S_1 and S_0–S_2 transitions are nearly orthogonally polarized; (b) the transition moments in *trans*1 and *trans*2 form a large angle, both for S_1 and S_2. Therefore, for the emission occurring from *trans*1, positive anisotropy values indicate that the initially excited species corresponds to either S_1(*trans*1) or S_2(*trans*2); negative anisotropy implies S_1(*trans*2) or S_2(*trans*1). We note, however, that for some unsymmetrically substituted porphycenes the situation may be more complicated; in particular, the transition moment directions in *trans*1 and *trans*2 need not form a large angle in S_1 or S_2. Such behavior, first discussed for 9-amino-2,7,12,17-tetraphenylporphycene,[19] was confirmed by calculations of the presently studied amino derivatives (Fig. S1–S3, ESI†). It makes the distinction between two *trans* tautomeric forms based on emission anisotropy rather difficult. On the other hand, the calculations indicate that the pattern of nearly orthogonal S_0–S_1 and S_0–S_2 transition moments is retained after amino substitution.

The theoretical predictions are in excellent agreement with the experiment (Fig. 1). Even though the calculations overestimate the $S_1 \leftarrow S_0$ and $S_2 \leftarrow S_0$ transition energies (as is also the case for bare **Pc**), the calculated absorption pattern matches exactly the observed one. The lowest transition is observed (in toluene) at 13 755 cm^{-1}; the next, more intense band is located at 14 760 cm^{-1}. Weak bands at 15 800 and 16 860 cm^{-1} are barely observed in absorption, but they can be readily detected by emission anisotropy and MCD. Finally, an intense transition is observed at 17 650 cm^{-1}. These three bands exhibit negative MCD signals, indicating that they belong to $S_2 \leftarrow S_0$ transitions. The negative emission anisotropy at 17 650 cm^{-1} leaves little doubt about the assignment to *trans*1. Since it is well known that the vibronic feature in the $S_2 \leftarrow S_0$ absorption in porphycenes is more intense than the 0-0 transition, the band at 17 650 is assigned to the vibronic feature of S_2(*trans*1). The energy difference between the $S_2 \leftarrow S_0$ bands observed at 17 650 and 16 860 cm^{-1}, 790 cm^{-1}, is in perfect agreement with theoretical prediction of the difference between $S_2 \leftarrow S_0$ transitions in *trans*1 and *trans*2. We therefore assign the band at 16 860 cm^{-1} to the vibronic feature of S_2(*trans*2). The determination of the positions of the electronic origin of S_2 in *trans*1 and *trans*2 is not straightforward, since both the MCD and anisotropy show complex character, indicating mixing of S_1 and S_2 spectral features from both tautomers. Assuming that the dominant vibronic features lie, similarly as in other porphycenes, about 900 cm^{-1} to the blue from the S_2 origin, we estimate the S_2(0-0) energies of *trans*1 and *trans*2 as 16 750 and 15 960 cm^{-1}, respectively. The latter value is close to the shoulder observed at 15 900 cm^{-1} in the MCD spectrum. Regarding the former, it is difficult to find a spectral feature that would clearly correlate with this value. The negative MCD indicates the S_2 origin. Small positive anisotropy values in this spectral region suggest contributions from both, the origin of S_2(*trans*1) and the vibronic features of S_1(*trans*2).

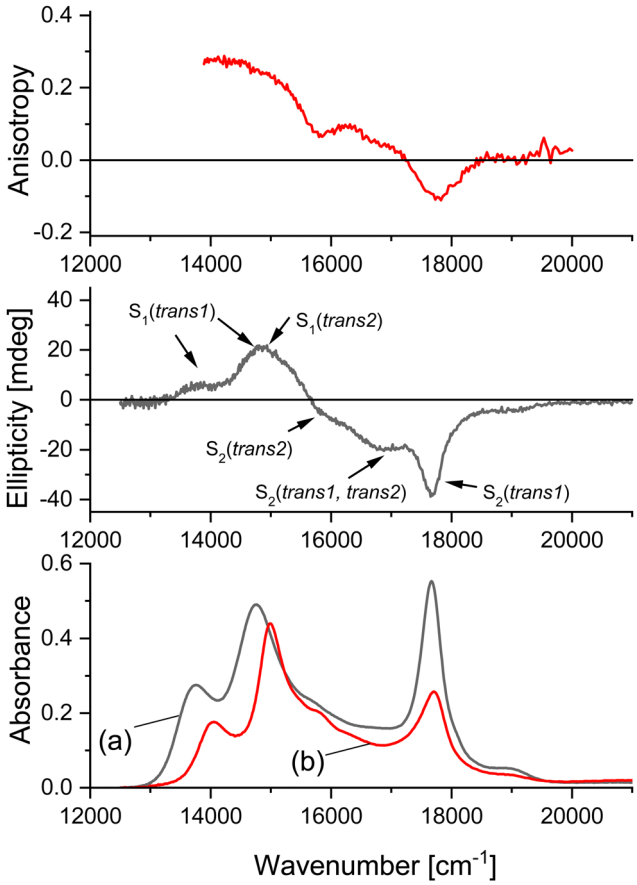

Fig. 1 Bottom, absorption of **APc** in toluene (a) and of **ttAPc** in paraffin (b). Middle, MCD of **APc** in toluene. Top, anisotropy of fluorescence excitation of **ttAPc** in paraffin, monitored at 735 nm.

In conclusion, we assign the bands observed at 13 755 and 14 760 cm^{-1} to the origins of transitions to S_1 in *trans*1 and *trans*2 forms, respectively. The corresponding values for S_2 are 16 750 and 15 900 cm^{-1}. The least accurate is the value of 16 750 cm^{-1}; we estimate that the maximum error in this assignment should not exceed ±200 cm^{-1}.

As mentioned below, these assignments are in perfect agreement with the calculated S_1–S_2 energy splittings. An observation that strongly reinforces the assignments is a much higher MCD intensity in *trans*2 than in *trans*1, an effect clearly seen in the comparison of relative absorption and MCD intensities of the bands at 16 860 and 17 650 cm^{-1}. It is caused by the smaller S_1–S_2 energy separation in *trans*2, which leads to a larger MCD signal. A similar effect has been recently reported for 9-fluoroporphycene.[22]

Our assignments agree with the results of a theoretical paper in which the absorption of 9-amino-2,6,12,17-tetraphenylporphycene

Table 4 Calculated transition energies (cm^{-1}) and oscillator strengths (in parentheses) of the tautomeric forms of **ttPc**, **ttAPc**, and **ttNPc**

	$S_1 \leftarrow S_0$[a]	$S_1 \rightarrow S_0$[b]	$S_2 \leftarrow S_0$[a]
ttPc			
trans	17 539 (0.15)	16 496 (0.18) 16 180 (0.23)	18 564 (0.26)
cis	17 493 (0.15)	16 314 (0.18) 16 209 (0.24)	18 635 (0.25)
ttAPc			
*trans*1	15 837 (0.21)	14 588 (0.21) 14 208 (0.26)	18 548 (0.20)
*trans*2	16 786 (0.31)	15 826 (0.30) 15 692 (0.41)	17 868 (0.11)
*cis*1	16 991 (0.26)	15 903 (0.24) 15 833 (0.36)	18 118 (0.16)
*cis*2	15 816 (0.21)	14 352 (0.21) 13 889 (0.26)	18 162 (0.18)
ttNPc			
*trans*1	16 543 (0.12)	13 283 (0.11) 13 665 (0.18)	17 421 (0.13)
*trans*2	16 373 (0.12)	14 015 (0.13) 14 074 (0.19)	17 914 (0.26)
*cis*1	16 260 (0.13)	13 930 (0.14) 14 132 (0.21)	17 831 (0.24)
*cis*2	16 437 (0.11)	13 807 (0.11) 14 295 (0.16)	17 928 (0.10)

[a] Optimized S_0 geometry. [b] Optimized S_1 geometry, first row: B3LYP/6-31+G(d,p), second row: CAM-B3LYP/6-31+G(d,p).

has been modelled using the nuclear ensemble method.[49] The authors concluded that the first absorption band originates from *trans*1, but the second band is dominated by transition from *trans*2.

DFT calculations performed for **ttAPc** (Table 4) yield a pattern very similar to that obtained for **APc**. The experiment (Fig. 1 and Fig. S4, ESI†) confirms the strong similarity of absorption and MCD in the two molecules. The tetra-*t*-butyl derivative exhibits in S_1 a small blue shift with respect to **APc** for both *trans* forms. In S_2, a red shift is observed for *trans*2, whereas for *trans*1 the transition energy remains the same within experimental error. Except for the latter, these shifts are correctly predicted by calculations. We assign the transitions observed in toluene at 14 000 and 17 650 cm^{-1} to the S_1 and S_2 transitions in *trans*1, whereas the corresponding bands in *trans*2 are located at 14 915 and 16 950 cm^{-1}. Based on the analysis carried out for **APc**, the S_2 values most likely correspond to the vibronic features.

Absorption of **tprAPc** strongly resembles that of **ttAPc**; the positions of the main bands differ by $\sim$100 cm^{-1} or less (Fig. S4, ESI†); such behavior is also predicted by calculations (Table S2, ESI†). The intensity ratio of the bands assigned to S_1(*trans*2) and S_2(*trans*1) increases somewhat in the order: **APc**, **tprAPc**, **ttAPc**, suggesting a slightly higher population of *trans*2 in the alkylated derivatives. In **APc**, the population of *trans*2 seems to increase in a polar solvent, as indicated by the relative increase of the 16 860 cm^{-1} peak, assigned to S_2(*trans*2). The intensity of this transition is stronger in acetonitrile and methanol than in toluene or *n*-hexane.

Nitroporphycenes. Theory predicts that, similarly as in aminoporphycenes, the lowest energy structures correspond to two nearly degenerate *trans* tautomers, with *trans*2 now being slightly more stable (Tables 1 and 2, Fig. S1, ESI†). The replacement of the amino by the nitro group leads to the reversal in the relative transition energies in the two forms (Tables 3 and 4, Fig. S2, ESI†). The lowest energy now corresponds to the *trans*2 species, whereas the $S_1 \leftarrow S_0$ origin in *trans*1 is calculated to lie 535 cm^{-1} higher. These predictions agree with the experiment (Fig. 2 and Fig. S5, ESI†): in both, absorption and MCD spectra a shoulder appears around 15 300 cm^{-1}, followed by the maximum at 15 810 (in toluene). The same pattern is observed in acetonitrile solution. The anisotropy of fluorescence excitation rapidly decreases between 15 300 and 15 810 cm^{-1}, corroborating the assignment of these two bands to the S_1 transition in two different tautomeric forms.

The S_2 assignment is more challenging. Two peaks are observed at 16 475 and 17 650 cm^{-1}. Both exhibit a negative MCD signal, indicating that they correspond to S_2. The same pattern is observed in bare porphycene, where the higher energy peak corresponds to the vibrational feature of the $S_2 \leftarrow S_0$ transition.[47] In fact, except for low energy shoulder in **NPc**, absorption spectra of **Pc** and **NPc** are very similar with respect to the location and intensity of the bands.

Absorption spectra of **tprNPc** and **ttNPc** are analogous to that of **NPc** (Fig. S5, ESI†). The bands in the spectra of **ttNPc** are

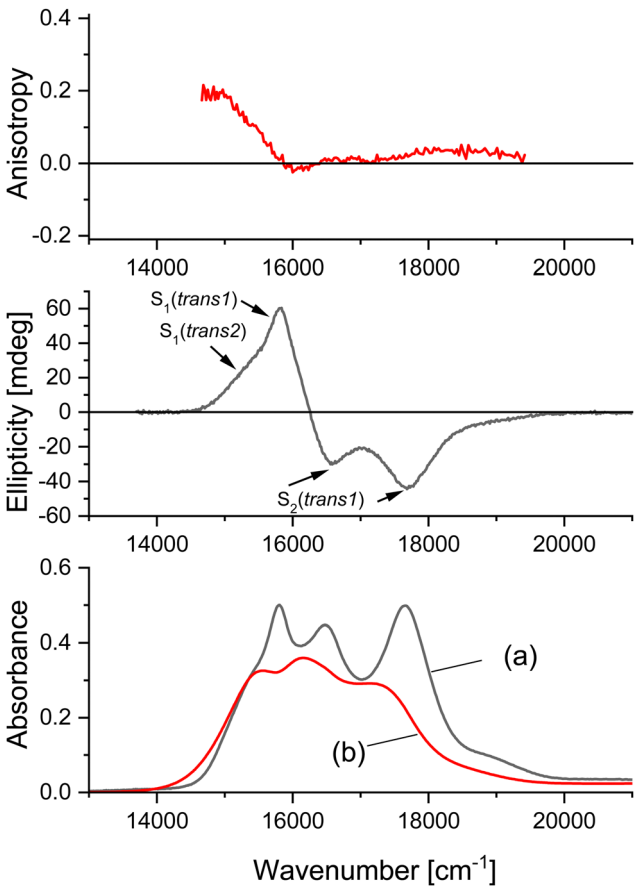

Fig. 2 Bottom, absorption of **NPc** in toluene (a) and of **ttNPc** in paraffin (b). Middle, MCD of **NPc** in toluene. Top, anisotropy of fluorescence excitation of **ttNPc** in paraffin, monitored at 710 nm.

distinctively broader than in **NPc** and **tprNPc**, but the overall shape remains similar. The low energy shoulder, visible in **NPc**, is not observed, in agreement with calculations that predict that in **ttNPc** the S_1 origins of *trans*1 and *trans*2 forms are spaced by less than 200 cm^{-1}. The experiment also confirms the theoretically predicted red shifts of transition energies in the *t*-butyl derivative.

Fig. 3 summarizes the $S_1 \leftarrow S_0$ and $S_2 \leftarrow S_0$ transition energies obtained experimentally and predicted by theory. It is evident that nitro and amino substitutions lead to different spectral patterns and excited states ordering. The lowest energy transition corresponds to *trans*1 in the amino and to *trans*2 in the nitro derivatives. In aminoporphycenes, the S_1–S_2 energy gap is larger in *trans*1 than in *trans*2, whereas the opposite occurs in nitroporphycenes. It should be recalled that the reversal of relative tautomer energies is predicted also for the ground electronic state, but the effect becomes much stronger upon excitation (Table 1). Based on the predicted relative energies in the *trans*1 and *trans*2 forms, one could expect the dominance of only one tautomer in S_1. As shown below, this is indeed the case, but, since in S_0 the other species is also present, the dynamics of its conversion into the lower energy form should also be observed.

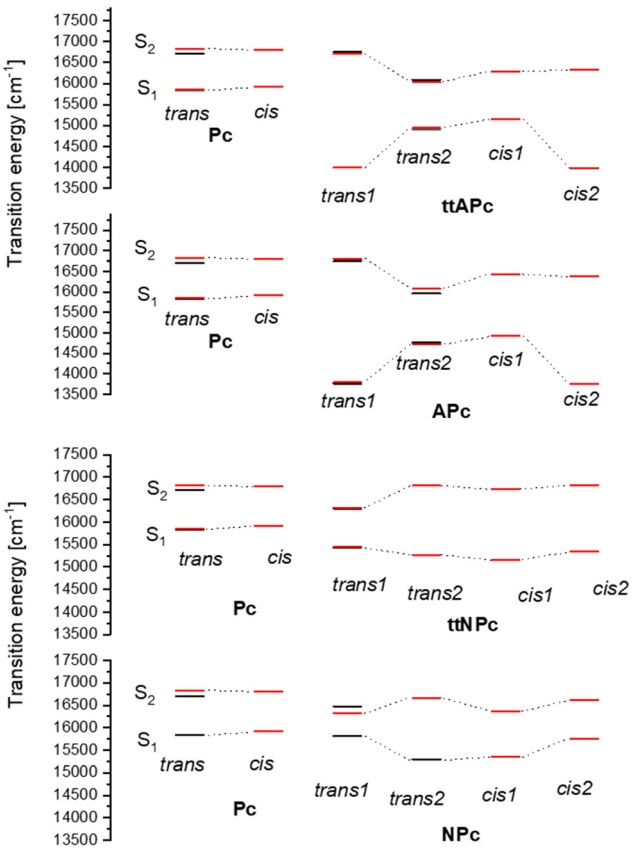

Fig. 3 Comparison of calculated (red bars) and experimentally observed (black bars) $S_1 \leftarrow S_0$ and $S_2 \leftarrow S_0$ transition energies in different tautomeric forms of **Pc** and its amino and nitro derivatives. The calculated values (see Tables 3 and 4) have been shifted to lower energies, so that the experimental and calculated values of the S_0–S_1 transition coincide within less than 50 cm^{-1}.

Aminoporphycenes. Samples of **APc**, **tprApc**, and **ttAPc**, measured several weeks after the synthesis, exhibit a similar, complicated fluorescence pattern (Fig. 4). To facilitate comparison with the literature data, we present the emission spectra in the wavelength scale. The main, most intense fluorescence (F_1) in **APc** has a maximum at 727, 749, 756, and 762 nm in *n*-hexane, toluene, acetonitrile, and methanol, respectively. In addition to F_1, two bands of weak intensity appear at higher energies, peaking (in acetonitrile) at 668 nm (F_2) and 635 nm (F_3). The F_1/F_2 and F_2/F_3 intensity ratios depend on solvent and excitation wavelength, indicating that these emissions occur from different species. The excitation spectrum of F_1 practically coincides with the absorption. The excitation spectra of F_2 and F_3 look similar, but the former is red-shifted by *ca.* 20 nm (Fig. S6, ESI†). Both spectra exhibit typical features of porphycene absorption.

Previous studies of derivatives of 9-aminoporphycene, substituted at the β positions with phenyl, propyl or methoxyethyl groups,[44,45] reported F_1 and F_2 (but not F_3) emissions of comparable intensity. These emissions were assigned to *trans*1 and *trans*2 tautomers, respectively. Our present results suggest a different interpretation. We noticed that for freshly prepared samples (measured one or two days after synthesis or just after sample purification by chromatography), the F_2 and F_3 emissions are barely observable. However, their intensity steadily grows with time (Fig. S7, ESI†) and, for samples that are a few weeks old, F_2 and F_3 bands become (for certain excitation wavelengths) comparable or even stronger than F_1. These results leave no doubts that F_2 and F_3 do not originate from **APc**. The final proof was provided by applying chromatography for a sample of **tprAPc**. In addition to the main spot, two other ones were observed on the chromatographic plate. Fluorescence spectra recorded for the species present in these additional spots coincided with F_2 and F_3 emissions. In a separate HPLC experiment carried out for **APc**, we separated, in addition to the main component, two other species, each of them showing single emission corresponding to F_2 and F_3. We conclude that the previous assignment of F_2 emission in aminoporphycenes to the *trans*2 tautomer has to be abandoned. Regarding F_1, the assignment to *trans*1 seems safe. Still, time-resolved measurements reported below show that the high energy portion of F_1 contains a fraction of short-lived fluorescence from *trans*2.

All three aminoporphycenes exhibited qualitatively the same behavior, but the appearance of F_2 and F_3 was significantly slower in the alkylated derivatives than in **APc**. We also noticed that F_3/F_2 ratio seemed to be smaller in nonpolar toluene or paraffin than in polar acetonitrile. The origin of the species responsible for F_2 and F_3 is now under investigation and will be a subject of a separate article.

When excited into the lowest energy absorption band, the F_1 decay in **APc** is monoexponential (2.6 ± 0.1 ns in *n*-hexane, 2.00 ± 0.05 ns in toluene, 1.40 ± 0.05 ns in acetonitrile, and 1.00 ± 0.05 ns in methanol). Similar behavior was found for **tprAPc** (2.40 ± 0.05 ns in toluene, 1.90 ± 0.05 ns in acetonitrile). When

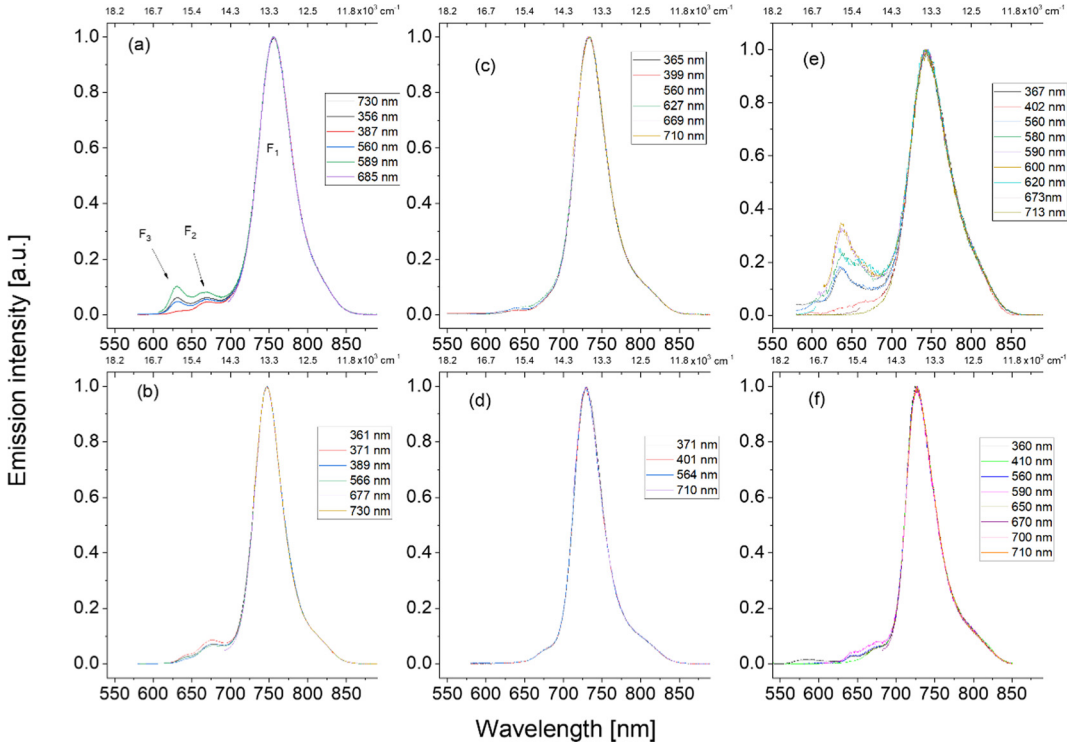

Fig. 4 Room temperature fluorescence spectra: **APc** (a), **tprAPc** (c), and **ttAPc** (e) in acetonitrile, **APc** (b) and **tprAPc** (d) in toluene, and **ttAPc** (f) in paraffin. The spectra were normalized to the F_1 maximum. Excitation wavelengths have been color-coded.

the fluorescence was probed at its high energy edge (670 nm), both molecules demonstrated the same kinetic feature (Fig. S8 and S9, ESI†): in addition to the main component, identical to that obtained for monitoring the low energy part, a short decay was found, indicating a rapid excited state transformation. It is natural to assign this component to *trans*2 → *trans*1 tautomerization, since *trans*2, upon excitation, is destabilized with respect to *trans*1. Such interpretation allows to explain the coincidence of F_1 excitation spectrum with that of absorption (which contains contributions from *trans*1, *trans*2, and, possibly, also *cis*1). The unusual behavior results from the fact that most of the excited population finally ends in the S_1 state of *trans*1, which emits the dominant fluorescence.

The behavior of **ttAPc** is qualitatively similar to that of **APc** and **tprAPc**, but the fluorescence quantum yield is lower (Table 5) and the decay time is shorter. Interestingly a large difference is found between the decay times in toluene (0.15 ± 0.03 ns) and paraffin (1.01 ± 0.05 ns). The longer decay in more viscous solvent indicates a radiationless channel involving a large amplitude motion, such as distortion from planarity. Similar viscosity dependence has been reported for other porphycenes.[20]

Table 5 Fluorescence quantum yields (293 K). For aminoporphycenes, the values are calculated from F_1 emission only

	Solvent	ϕ_{fl}[a]
APc	Toluene	0.03
	Acetonitrile	0.01
tprAPc	Toluene	0.04
	Acetonitrile	0.02
ttAPc	*n*-Hexane	3.6×10^{-3}
	Acetonitrile	6×10^{-4}
NPc	Toluene	0.10
	Acetonitrile	0.06
tprNPc	Toluene	0.03
	Acetonitrile	0.009
ttNPc	*n*-Hexane	4×10^{-4}
	Toluene	3×10^{-4}
	Acetonitrile	6×10^{-4}
	Ethanol	3×10^{-4}
	DMSO	5×10^{-4}

[a] Estimated maximum error: ±20% for $\phi_{fl} > 10^{-2}$, ±30% for lower values.

Nitroporphycenes. NPc emits fluorescence (Fig. 5) peaking at 669 nm in toluene and 665 nm in acetonitrile. The spectral shift to the blue with increasing solvent polarity is in line with the absorption (Fig. S5, ESI†). Fluorescence excitation spectra coincide with the absorption. The emission decay is monoexponential and becomes faster with increasing solvent polarity. The values of fluorescence lifetimes obtained at room temperature are: 4.4 ± 0.2 ns (*n*-hexane), 3.4 ± 0.2 ns (toluene), 2.7 ± 0.2 ns (acetonitrile), and 2.2 ± 0.1 ns (acetonitrile : water 80 : 20 v/v).

The emission of **ttNPc** is shifted to the blue with respect to **NPc** (by about 15 nm). The quantum yield is extremely low: the **NPc**:**ttNPc** intensity ratio is ~200 (Table 5). The decay time, a few tens of picoseconds, was too short to be accurately measured with our setup. We also observed that the shape of the emission varies somewhat for different excitation wavelengths. This may indicate the presence of various conformers, but we cannot exclude contribution from impurities, since the

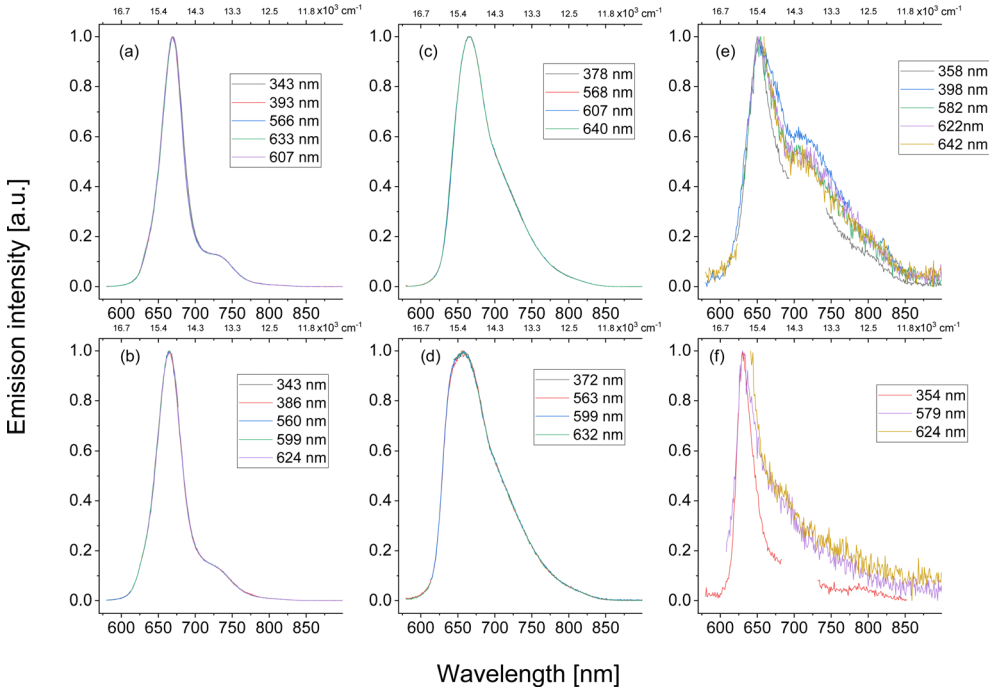

Fig. 5 Room temperature fluorescence spectra: **NPc**, **tprNPc**, and **ttNPc** in toluene (a, c and e) and acetonitrile (b, d and f). Excitation wavelengths have been color-coded.

fluorescence of **ttNPc** is extremely weak, which precludes reliable analysis of excitation spectra monitored at different emission wavelengths.

Discussion

Absorption spectra

The large difference between the absorption spectra of amino and nitroporphycenes can be understood using the calculated pattern of frontier electronic orbitals (Fig. 6). Substitution of porphycene with the electron donating amino moiety results in the destabilization of orbital energies; the strongest effect is induced in the HOMO−1 orbital, which has the largest LCAO coefficient at position 9. The other occupied orbital is only weakly affected, as it has a node at this position. In consequence, the two occupied orbitals, nearly degenerate in parent **Pc**, become split in **APc** by a significant amount, 0.4 eV. In addition, their ordering is reversed, as the more affected, destabilized orbital (HOMO in **APc**) corresponds to HOMO−1 in **Pc**.

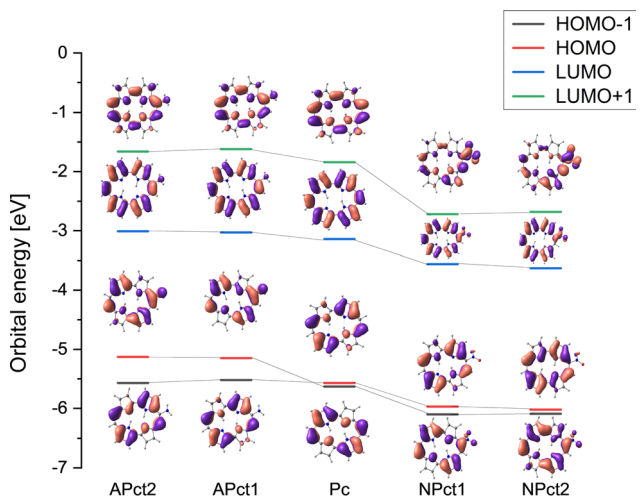

Fig. 6 Calculated frontier orbital energy patterns. Suffixes t1 and t2 indicate *trans*1 and *trans*2 tautomers, respectively.

Substitution by the electron-accepting nitro group leads to the stabilization of all the orbitals. The most affected orbitals are the unoccupied ones, but the HOMOs also shift to lower energies. The energy ordering is not inverted, and the spacing increases in comparison with **Pc**. Still, the effect is much weaker than in **APc**, resulting in the observed S_1–S_2 splittings of 665 cm^{-1} in *trans*1 and 1500 cm^{-1} in *trans*2.

The above analysis explains the increasing spectral range of the Q absorption upon passing from **Pc** to **NPc** and **APc**. One should note that simple consideration of orbital energies cannot account for different splittings of transition energies in *trans*1 and *trans*2. On the other hand, DFT calculations accurately reproduce the experimental results (Fig. S10, ESI†).

Photophysical properties

The radiative rate constant of S_1 depopulation in **Pc** has been previously measured for different solvents. After correction for the square of the refractive index, the same value of $(2.3 \pm 0.1) \times 10^7$ s^{-1} is obtained for each solvent.[24] We obtained practically the same values for *n*-hexane solutions of **APc** $(2.3 \pm 0.2) \times 10^7$ s^{-1} and **NPc** $(1.9 \pm 0.2) \times 10^7$ s^{-1}. On the other hand, the sum of nonradiative rate constants in **APc** $(3.4 \pm 0.4) \times 10^8$ s^{-1}

and **NPc** $(1.8 \pm 0.2) \times 10^8$ s^{-1} is definitely higher than in **Pc** $(5.7 \pm 0.6) \times 10^7$ s^{-1}. The radiative rate constants do not seem to change significantly in the alkyl derivatives, but a large increase of nonradiative deactivation rate is observed for **ttAPc** (about an order of magnitude) and **ttNPc** (more than two orders of magnitude). Sevenfold difference in the fluorescence lifetimes measured for **ttAPc** in toluene (0.15 ns) and paraffin (1.01 ns) indicates that the efficient nonradiative process may be associated with geometry changes in S_1, an effect reported for other porphycenes.[24] In order to analyze this process in more detail, we compare the optimized geometries in the ground and lowest excited singlet states. The macrocycle of **NPc** is predicted to be planar in S_0 and S_1 (Fig. S11, ESI†). However, the NO_2 plane forms an angle of 38° (*trans*1) or 30° (*trans*2) with the plane of the macrocycle. Upon excitation to S_1, coplanarity is predicted for *trans*2, which is also the emitting form. Interestingly, *trans*1 retains its S_0 structure in the S_1 state. Introduction of *t*-butyl substituents that leads to **ttNPc** (Fig. S12, ESI†) induces nonplanarity already in S_0, but the distortion becomes much larger in S_1. In both states, the effect is stronger in *trans*1.

For **APc**, planar macrocycle is obtained for both S_0 and S_1, with a slightly less pyramidalized amino group in the excited state (Fig. S13, ESI†). **ttAPc** is slightly nonplanar in S_0. The distortion increases in S_1 and consists of the deviation of the pyrrole ring closest to the amino group from the macrocycle plane (Fig. S14, ESI†). The effect is definitely stronger for the (emitting) *trans*1 tautomer.

The above results show that the huge decrease in fluorescence quantum yield in **ttNPc** is associated with steric interactions between *t*-butyl and nitro moieties. In agreement with experiment, a similar, but less pronounced effect is expected for **ttApc**. The finding that geometry distortions are different for different tautomers brings up an interesting issue: the possibility of influencing the tautomerization rate by changing the rigidity of the environment.

We finally note that, upon geometry optimization of the S_1 state of the *cis*3 form, a conical intersection was found for both **ttAPc** and **ttNPc**, which may explain the low emission intensity.

Tautomeric equilibria

Photophysical studies demonstrate that both, amino and nitroporphycenes behave similarly to other unsymmetrically substituted porphycenes, such as 9-acetoxy[18,50] or 9-fluoro[22] derivatives. In the ground electronic state, two *trans* tautomers of similar energy coexist, whereas in S_1 the equilibrium is shifted towards the structure which was already more stable in S_0 (*trans*1 in amino-, *trans*2 in nitroporphycenes).

Excited state tautomerization is a unidirectional ''downhill'' process leading to the most stable form. Determination of the rates requires techniques with better time resolution than used in the present work; we estimate, based on the value of the fast component appearing in the emission probed at its blue edge, that the double hydrogen transfer in S_1 takes a few tens of picoseconds.

The mechanisms of tautomerization can be quite complex. In the ground electronic states, three different pathways should be considered for *trans*2 → *trans*1 conversion. The first two involve *cis*1 and *cis*2 as intermediates in the stepwise process. The third is the concerted asynchronous transfer of two hydrogens; a synchronous process is very unlikely due to lack of symmetry. In the lowest excited singlet state, tautomerization may be even more complicated, possibly involving high energy *cis*3 and *cis*4 species, because their energy is calculated as being close to that of the S_1 energies of the other four species.

The calculations (Fig. 7) indicate similar barriers for stepwise *trans*1–*trans*2 conversions involving either *cis*1 or *cis*2 in the ground electronic state of both **APc** and **NPc**. The barrier for the first step is always higher than for the second one. This is also true for S_1. This means that the experimental observation of the *cis* form (which would demonstrate a stepwise mechanism) may be difficult, as the decay of this intermediate species would be faster than its formation.

The barriers for concerted transfer are about 50% higher than those obtained for the stepwise process. A similar pattern was obtained for **Pc** and its other symmetrically substituted derivatives. However, the experimental evidence in the case of **Pc** favors the concerted mechanism, involving activation of a specific, low frequency vibrational mode.[12] It remains to be checked whether the symmetry lowering in amino and nitro derivatives leads to the change in the tautomerization path. It seems likely, since the calculations predict that the two intramolecular H-bonds are no longer equivalent. The difference between the HB strengths is both substituent- and tautomer-specific. It can also vary between S_0 and S_1. For instance, in the ground electronic state of *trans*1 tautomer of **APc**, the N21H···N24 HB is predicted to be stronger than the other one, N22H···N23, as evidenced by the calculated values of the NH stretching frequencies, 2917 and 2944 cm^{-1}, respectively. The opposite occurs for *trans*2 (2861 *vs.* 2844 cm^{-1}). Electronic excitation enhances these patterns: the S_1 frequencies calculated for *trans*1 are 2945 and 3090 cm^{-1}, whereas for *trans*2 we obtain 2894 and 2761 cm^{-1}. For the *trans*1 tautomer of **NPc**, the S_0 frequencies are 2876 and 2973 cm^{-1}, whereas the S_1 calculation yields the values of 2923 and 2999 cm^{-1}. Thus, contrary to the case of **APc**, the difference between the two HBs decreases in S_1. Finally, in the *trans*2 form of **NPc**, the two HBs are different in S_0 (2892 *vs.* 2848 cm^{-1}), but in S_1 both protons participate in the antisymmetric and symmetric combinations of NH stretches, separated by only 2 cm^{-1} (2911 and 2913 cm^{-1}, respectively). This result suggests an attractive possibility to switch from stepwise to concerted tautomerization mechanism by a suitable combination of structure, tautomeric form, and electronic state.

However, the predictive power of calculations of unsymmetrical porphycenes seems to be lower than in the case of symmetrical derivatives. In particular, the correlation between the parameters that characterize the HB strength, which has been very useful for symmetrically substituted porphycenes,[13] becomes rather weak. As an example, the plot of calculated NH stretching frequencies *vs.* the N–N distances (Fig. S15, ESI†) shows that for practically the same N–N separation (266.1–266.3 pm), frequencies that differ by more than 200 cm^{-1} are

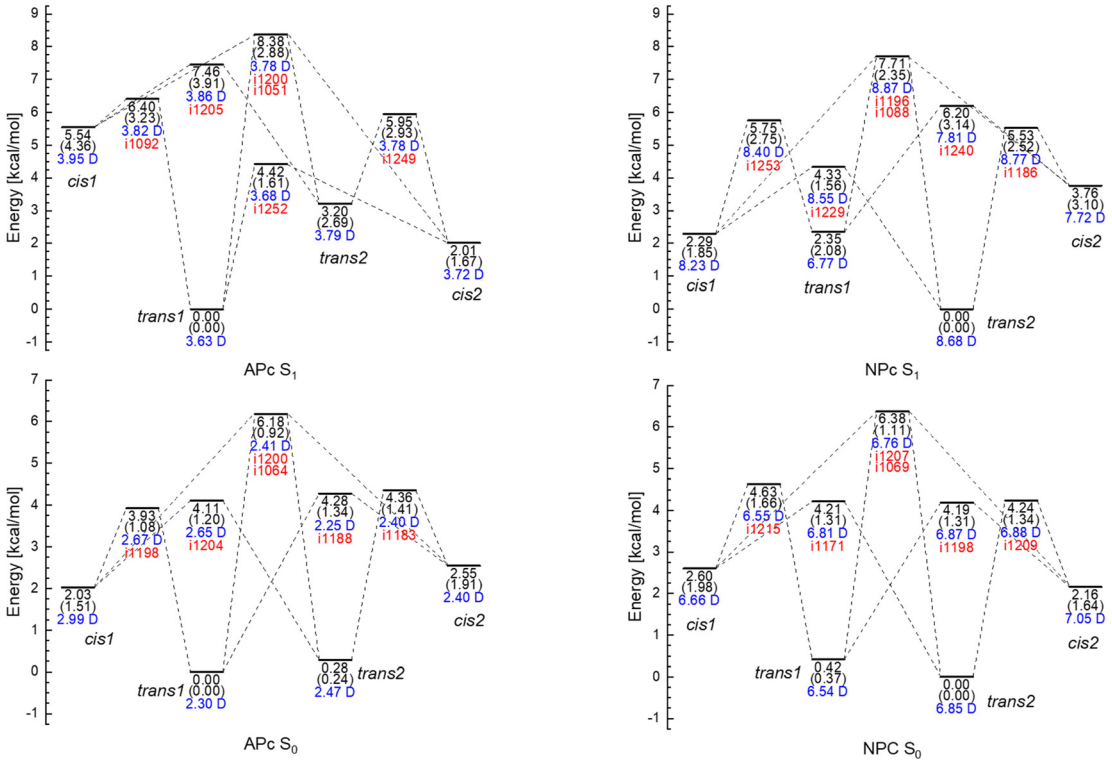

Fig. 7 Calculated relative energies (kcal mol^{-1}) of four tautomeric forms of **APc** (left) and **NPc** (right) in the ground (bottom) and lowest excited singlet (top) states, and of the transition states involved in tautomerization. In parentheses, zero-point-vibrational-energy corrected values. In red, imaginary frequencies (cm^{-1}); in blue, calculated permanent dipole moments (D).

obtained. Evidently, the distance between the HB donor and acceptor is no longer a good index when the electron density distribution is not symmetrical. This is true even when considering two HBs of the same tautomeric form in the same electronic state.

Summary and conclusions

Substitution of porphycene at the *meso* position with the amino or nitro group leads to spectral changes that can be rationalized by the shifts of frontier orbital energies caused by electron donating or accepting moieties. The spacing between S_1 and S_2 states, *ca.* 900 cm^{-1} in unsubstituted **Pc**, increases to 3000 cm^{-1} in the *trans*1 form of **APc** and to 1500 cm^{-1} in the *trans*2 tautomer of **NPc**. For the other *trans* species the S_2–S_1 separation is about two times smaller in both, amino and nitro derivatives.

Two *trans* tautomers of similar energies coexist in the ground state. Upon electronic excitation, one form (*trans*1 in **APc**, *trans*2 in **NPc**) is strongly stabilized with respect to the other. The least stable species rapidly converts into the lower energy one. As a result, fluorescence occurs mainly from one tautomeric form. Support for one-way rapid excited state *trans*–*trans* conversion is provided by a fast-decaying component in the blue part of the emission.

APc and **NPc**, as well as their 2,7,12,17-tetrapropyl derivatives emit with moderate quantum yields, but fluorescence becomes very weak for tetra-*t*-butyl substituted porphycenes. The effect is the strongest for the nitro derivative and is most likely caused by the steric repulsion between the nitro and *t*-butyl moieties.

The two classes of porphycenes studied in this work are attractive models for more detailed studies of ground and excited state tautomerization mechanisms. Unfortunately, such investigation may be difficult to perform because of instability, which is a problem especially in the case of aminoporphycenes. Our ongoing studies focus on the identification of the species produced both in the dark and after photoirradiation.

Data availability

The data that support the findings of this study are available from the corresponding author upon reasonable request.

Conflicts of interest

There are no conflicts to declare.

Acknowledgements

This work was supported by the Polish National Science Center, grant 2016/22/A/ST4/00029, and by the grants from the PL-Grid infrastructure and the Interdisciplinary Centre for

Mathematical and Computational Modeling for a computing grant (grant no. G17-14).

References

1 E. Vogel, M. Köcher, H. Schmickler and J. Lex, Porphycene - a novel porphin isomer, *Angew. Chem., Int. Ed. Engl.*, 1986, **25**, 257–259.
2 J. C. Stockert, M. Cañete, A. Juarranz, A. Villanueva, R. W. Horobin, J. Borrell, J. Teixidó and S. Nonell, Porphycenes: facts and prospects in photodynamic therapy of cancer, *Curr. Med. Chem.*, 2007, **14**, 997–1026.
3 L. Polo, A. Segalla, G. Bertoloni, G. Jori, K. Schaffner and E. Reddi, Polylysine–porphycene conjugates as efficient photosensitizers for the inactivation of microbial pathogens, *J. Photochem. Photobiol., B*, 2000, **59**, 152–158.
4 N. Masiera, J. Ostapko, A. Gorski, A. Bojarska, I. Gawryszewska, E. Sadowy, W. Hryniewicz and J. Waluk, Photoeradication of bacteria with porphycenes: substituent effects on the efficiency, *Eur. J. Med. Chem.*, 2020, **200**, 112472.
5 T. Matsuo, D. Murata, Y. Hisaeda, H. Hori and T. Hayashi, Porphyrinoid chemistry in hemoprotein matrix: detection and reactivities of iron(IV)-oxo species of porphycene incorporated into horseradish peroxidase, *J. Am. Chem. Soc.*, 2007, **129**, 12906–12907.
6 C. M. Che, H. F. Xiang, S. S. Y. Chui, Z. X. Xu, V. A. L. Roy, J. J. Yan, W. F. Fu, P. T. Lai and I. D. Williams, A high-performance organic field-effect transistor based on platinum(II) porphyrin: peripheral substituents on porphyrin ligand significantly affect film structure and charge mobility, *Chem. – Asian J.*, 2008, **3**, 1092–1103.
7 T. Hayashi, K. Okazaki, N. Urakawa, H. Shimakoshi, J. L. Sessler, E. Vogel and Y. Hisaeda, Cobaltporphycenes as catalysts. The oxidation of vinyl ethers via the formation and dissociation of cobalt–carbon bonds, *Organometallics*, 2001, **20**, 3074–3078.
8 W. C. Lo, C. M. Che, K. F. Cheng and T. C. W. Mak, Catalytic and asymmetric cyclopropanation of styrenes catalysed by ruthenium porphyrin and porphycene complexes, *Chem. Commun.*, 1997, 1205–1206.
9 A. Berlicka and B. König, Porphycene-mediated photooxidation of benzylamines by visible light, *Photochem. Photobiol. Sci.*, 2010, **9**, 1359–1366.
10 K. Oohora, H. Meichin, L. Zhao, M. W. Wolf, A. Nakayama, J.-Y. Hasegawa, N. Lehnert and T. Hayashi, Catalytic Cyclopropanation by Myoglobin Reconstituted with Iron Porphycene: Acceleration of Catalysis due to Rapid Formation of the Carbene Species, *J. Am. Chem. Soc.*, 2017, **139**, 17265–17268.
11 M. Stępień, B. Donnio and J. L. Sessler, Discotic liquid-crystalline materials based on porphycenes: a mesogenic metalloporphycene-tetracyanoquinodimethane (TCNQ) adduct, *Chem. – Eur. J.*, 2007, **13**, 6853–6863.
12 J. Waluk, Spectroscopy and tautomerization studies of porphycenes, *Chem. Rev.*, 2017, **117**, 2447–2480.
13 P. Ciąćka, P. Fita, A. Listkowski, M. Kijak, S. Nonell, D. Kuzuhara, H. Yamada, C. Radzewicz and J. Waluk, Tautomerism in Porphycenes: Analysis of Rate-Affecting Factors, *J. Phys. Chem. B*, 2015, **119**, 2292–2301.
14 P. Ciąćka, P. Fita, A. Listkowski, C. Radzewicz and J. Waluk, Evidence for Dominant Role of Tunneling in Condensed Phases and at High Temperatures: Double Hydrogen Transfer in Porphycenes, *J. Phys. Chem. Lett.*, 2016, **7**, 283–288.
15 M. Gil, J. A. Organero, J. Waluk and A. Douhal, Ultrafast dynamics of alkyl-substituted porphycenes in solution, *Chem. Phys. Lett.*, 2006, **422**, 142–146.
16 M. Gil and J. Waluk, Vibrational gating of double hydrogen tunneling in porphycene, *J. Am. Chem. Soc.*, 2007, **129**, 1335–1341.
17 P. Fita, N. Urbańska, C. Radzewicz and J. Waluk, Ground and excited state tautomerization rates in porphycenes, *Chem.– Eur. J.*, 2009, **15**, 4851–4856.
18 P. Fita, P. Garbacz, M. Nejbauer, C. Radzewicz and J. Waluk, Ground and excited state double hydrogen transfer in symmetric and asymmetric potentials: comparison of 2,7,12,17-tetra-*n*-propylporphycene with 9-acetoxy-2,7,12,17-tetra-*n*-propylporphycene, *Chem. – Eur. J.*, 2011, **17**, 3672–3678.
19 P. Fita, M. Pszona, G. Orzanowska, D. Sánchez-García, S. Nonell, E. Vauthey and J. Waluk, Tautomerization in 2,7,12,17-tetraphenylporphycene and 9-amino-2,7,12,17-tetraphenylporphycene: influence of asymmetry on the transition moment directions, *Chem. – Eur. J.*, 2012, **18**, 13160–13167.
20 M. Gil, J. Dobkowski, G. Wiosna-Sałyga, N. Urbańska, P. Fita, C. Radzewicz, M. Pietraszkiewicz, P. Borowicz, D. Marks, M. Glasbeek and J. Waluk, Unusual, solvent viscosity-controlled tautomerism and photophysics: *meso*-alkylated porphycenes, *J. Am. Chem. Soc.*, 2010, **132**, 13472–13485.
21 P. Kasprzycki, P. Kopycki, A. Listkowski, A. Gorski, C. Radzewicz, D. J. S. Birch, J. Waluk and P. Fita, Influence of local microenvironment on the double hydrogen transfer in porphycene, *Phys. Chem. Chem. Phys.*, 2020, **22**, 17117–17128.
22 A. Listkowski, A. Kharchenko, P. Ciąćka, M. Kijak, N. Masiera, R. Rybakiewicz, R. Luboradzki, P. Fita and J. Waluk, Fluorinated Porphycenes: Synthesis, Spectroscopy, Photophysics, and Tautomerism, *ChemPlusChem*, 2020, **85**, 2197–2206.
23 A. Listkowski, N. Masiera, M. Kijak, R. Luboradzki, B. Leśniewska and J. Waluk, Controlling Emissive Properties by Intramolecular Hydrogen Bonds: Alkyl and Aryl *meso*-Substituted Porphycenes, *Chem. – Eur. J.*, 2021, **27**, 6324–6333.
24 M. Kijak, K. Nawara, A. Listkowski, N. Masiera, J. Buczyńska, N. Urbańska, G. Orzanowska, M. Pietraszkiewicz and J. Waluk, 2 + 2 Can Make Nearly a Thousand! Comparison of Di- and Tetra-*Meso*-Alkyl-Substituted Porphycenes, *J. Phys. Chem. A*, 2020, **124**, 4594–4604.
25 E. T. Mengesha, A. Zehnacker-Rentien, J. Sepioł, M. Kijak and J. Waluk, Spectroscopic Study of Jet-Cooled Deuterated Porphycenes: Unusual Isotopic Effects on Proton Tunneling, *J. Phys. Chem. B*, 2015, **119**, 2193–2203.

26 A. Vdovin, J. Sepioł, N. Urbańska, M. Pietraszkiewicz, A. Mordziński and J. Waluk, Evidence for two forms, double hydrogen tunneling, and proximity of excited states in bridge-substituted porphycenes: supersonic jet studies, *J. Am. Chem. Soc.*, 2006, **128**, 2577–2586.
27 A. Vdovin, J. Waluk, B. Dick and A. Slenczka, Mode-selective promotion and isotope effects of concerted double-hydrogen tunneling in porphycene embedded in superfluid helium nanodroplets, *Chem. Phys. Chem.*, 2009, **10**, 761–765.
28 H. Piwoński, A. Sokołowski, M. Kijak, S. Nonell and J. Waluk, Arresting Tautomerization in a Single Molecule by the Surrounding Polymer: 2,7,12,17-Tetraphenylporphycene, *J. Phys. Chem. Lett.*, 2013, **4**, 3967–3971.
29 H. Piwoński, C. Stupperich, A. Hartschuh, J. Sepioł, A. Meixner and J. Waluk, Imaging of tautomerism in a single molecule, *J. Am. Chem. Soc.*, 2005, **127**, 5302–5303.
30 L. Piatkowski, C. Schanbacher, F. Wackenhut, A. Jamrozik, A. J. Meixner and J. Waluk, Nature of Large Temporal Fluctuations of Hydrogen Transfer Rates in Single Molecules, *J. Phys. Chem. Lett.*, 2018, **9**, 1211–1215.
31 A. Bednarz, I. Kamińska, A. Jamrozik, K. Zielonka, A. Listkowski and J. Waluk, Substituent screening effect on single-molecule photostability: comparison of three differently substituted porphycenes, *Methods Appl. Fluoresc.*, 2021, **9**, 035004.
32 S. Gawinkowski, M. Pszona, A. Gorski, J. Niedziółka-Jönsson, I. Kamińska, W. Nogala and J. Waluk, Single molecule Raman spectra of porphycene isotopologues, *Nanoscale*, 2016, **8**, 3337–3349.
33 M. Pszona, S. Gawinkowski, R. Jager, I. Kaminska and J. Waluk, Influence of bulky substituents on single-molecule SERS sensitivity, *J. Chem. Phys.*, 2022, **156**, 014201.
34 T. Kumagai, F. Hanke, S. Gawinkowski, J. Sharp, K. Kotsis, J. Waluk, M. Persson and L. Grill, Thermally and vibrationally induced tautomerization of single porphycene molecules on a Cu(110) surface, *Phys. Rev. Lett.*, 2013, **111**, 246101–246105.
35 T. Kumagai, F. Hanke, S. Gawinkowski, J. Sharp, K. Kotsis, J. Waluk, M. Persson and L. Grill, Controlling intramolecular hydrogen transfer in a porphycene molecule with single atoms or molecules located nearby, *Nat. Chem.*, 2014, **6**, 41–46.
36 J. Ladenthin, T. Frederiksen, M. Persson, J. Sharp, S. Gawinkowski, J. Waluk and T. Kumagai, Force-induced tautomerization in a single molecule, *Nat. Chem.*, 2016, **8**, 935–940.
37 M. Koch, M. Pagan, M. Persson, S. Gawinkowski, J. Waluk and T. Kumagai, Direct Observation of Double Hydrogen Transfer via Quantum Tunneling in a Single Porphycene Molecule on a Ag(110) Surface, *J. Am. Chem. Soc.*, 2017, **139**, 12681–12687.
38 J. N. Ladenthin, L. Grill, S. Gawinkowski, S. Liu, J. Waluk and T. Kumagai, Hot Carrier-Induced Tautomerization within a Single Porphycene Molecule on Cu(111), *ACS Nano*, 2015, **9**, 7287–7295.
39 T. Kumagai, J. Ladenthin, Y. Litman, M. Rossi, L. Grill, S. Gawinkowski, J. Waluk and M. Persson, Quantum tunneling in real space: tautomerization of single porphycene molecules on the (111) surface of Cu, Ag, and Au, *J. Chem. Phys.*, 2018, **148**, 102330.
40 H. Böckmann, S. Liu, J. Mielke, S. Gawinkowski, J. Waluk, L. Grill, M. Wolf and T. Kumagai, Direct Observation of Photoinduced Tautomerization in Single Molecules at a Metal Surface, *Nano Lett.*, 2016, **16**, 1034–1041.
41 D. Koga, T. Ono, H. Shinjo and Y. Hisaeda, Hydrogen Bond Engineering Visualized by Picometer-Level Distortion of Planar Porphyrin Isomers, *J. Phys. Chem. Lett.*, 2021, **12**, 10429–10436.
42 S. E. Braslavsky, M. Müller, D. O. Mártire, S. Pörting, S. G. Bertolotti, S. Chakravorti, G. Koç-Weier, B. Knipp and K. Schaffner, Photophysical properties of porphycene derivatives (18 π porphyrinoids), *J. Photochem. Photobiol., B*, 1997, **40**, 191–198.
43 O. Arad, N. Rubio, D. Sánchez-García, J. I. Borrell and S. Nonell, Asymmetric porphycenes: synthesis and photophysical properties of 9-substituted 2,7,12,17-tetraphenylporphycenes, *J. Porphyrins phthalocyanines*, 2009, **13**, 376–381.
44 M. Duran-Frigola, R. Tejedor-Estrada, D. Sánchez-García and S. Nonell, Dual fluorescence in 9-amino-2,7,12,17-tetraphenylporphycene, *Phys. Chem. Chem. Phys.*, 2011, **13**, 10326–10332.
45 O. Planas, R. Tejedor-Estrada and S. Nonell, Tautomerism and dual fluorescence in 9-substituted *n*-propyl- and methoxyethyl-porphycenes, *J. Porphyrins phthalocyanines*, 2012, **16**, 633–640.
46 M. Taneda, A. Tanaka, H. Shimakoshi, A. Ikegami, K. Hashimoto, M. Abe and Y. Hisaeda, Synthesis and characterizations of *meso*-disubstituted asymmetric porphycenes, *Tetrahedron Lett.*, 2013, **54**, 5727–5729.
47 A. Starukhin, E. Vogel and J. Waluk, Electronic Spectra in Porphycenes in Rare Gas and Nitrogen Matrices, *J. Phys. Chem. A*, 1998, **102**, 9999.
48 J. Waluk, M. Müller, P. Swiderek, M. Köcher, E. Vogel, G. Hohlneicher and J. Michl, Electronic States of Porphycenes, *J. Am. Chem. Soc.*, 1991, **113**, 5511–5527.
49 Z. G. Lan, S. Nonell and M. Barbatti, Theoretical Characterization of Absorption and Emission Spectra of an Asymmetric Porphycene, *J. Phys. Chem. A*, 2012, **116**, 3366–3376.
50 M. Gil, J. Jasny, E. Vogel and J. Waluk, Ground and excited state tautomerization in 9-acetoxy-2,7,12,17-tetra-*n*-propylporphycene, *Chem. Phys. Lett.*, 2000, **323**, 534.